**ICHEP94 Ref. GLS0740** **CLEO CONF 94-17**
**Submitted to PA 16,2 Pl 9,19** **July 19, 1994**

# New Decay Modes of the $\Lambda_c^+$ Charm Baryon

M. Bishai,[1] J. Fast,[1] E. Gerndt,[1] R.L. McIlwain,[1] T. Miao,[1] D.H. Miller,[1] M. Modesitt,[1] D. Payne,[1] E.I. Shibata,[1] I.P.J. Shipsey,[1] P.N. Wang,[1] M. Battle,[2] J. Ernst,[2] L. Gibbons,[2] Y. Kwon,[2] S. Roberts,[2] E.H. Thorndike,[2] C.H. Wang,[2] J. Dominick,[3] M. Lambrecht,[3] S. Sanghera,[3] V. Shelkov,[3] T. Skwarnicki,[3] R. Stroynowski,[3] I. Volobouev,[3] G. Wei,[3] P. Zadorozhny,[3] M. Artuso,[4] M. Gao,[4] M. Goldberg,[4] D. He,[4] N. Horwitz,[4] G.C. Moneti,[4] R. Mountain,[4] F. Muheim,[4] Y. Mukhin,[4] S. Playfer,[4] Y. Rozen,[4] S. Stone,[4] X. Xing,[4] G. Zhu,[4] J. Bartelt,[5] S.E. Csorna,[5] Z. Egyed,[5] V. Jain,[5] D. Gibaut,[6] K. Kinoshita,[6] P. Pomianowski,[6] B. Barish,[7] M. Chadha,[7] S. Chan,[7] D.F. Cowen,[7] G. Eigen,[7] J.S. Miller,[7] C. O'Grady,[7] J. Urheim,[7] A.J. Weinstein,[7] M. Athanas,[8] W. Brower,[8] G. Masek,[8] H.P. Paar,[8] M. Sivertz,[8] J. Gronberg,[9] R. Kutschke,[9] S. Menary,[9] R.J. Morrison,[9] S. Nakanishi,[9] H.N. Nelson,[9] T.K. Nelson,[9] C. Qiao,[9] J.D. Richman,[9] A. Ryd,[9] H. Tajima,[9] D. Sperka,[9] M.S. Witherell,[9] R. Balest,[10] K. Cho,[10] W.T. Ford,[10] D.R. Johnson,[10] K. Lingel,[10] M. Lohner,[10] P. Rankin,[10] J.G. Smith,[10] J.P. Alexander,[11] C. Bebek,[11] K. Berkelman,[11] K. Bloom,[11] T.E. Browder,[11*] D.G. Cassel,[11] H.A. Cho,[11] D.M. Coffman,[11] D.S. Crowcroft,[11] P.S. Drell,[11] D. Dumas,[11] R. Ehrlich,[11] P. Gaidarev,[11] R.S. Galik,[11] M. Garcia-Sciveres,[11] B. Geiser,[11] B. Gittelman,[11] S.W. Gray,[11] D.L. Hartill,[11] B.K. Heltsley,[11] S. Henderson,[11] C.D. Jones,[11] S.L. Jones,[11] J. Kandaswamy,[11] N. Katayama,[11] P.C. Kim,[11] D.L. Kreinick,[11] G.S. Ludwig,[11] J. Masui,[11] J. Mevissen,[11] N.B. Mistry,[11] C.R. Ng,[11] E. Nordberg,[11] J.R. Patterson,[11] D. Peterson,[11] D. Riley,[11] S. Salman,[11] M. Sapper,[11] F. Würthwein,[11] P. Avery,[12] A. Freyberger,[12] J. Rodriguez,[12] S. Yang,[12] J. Yelton,[12] D. Cinabro,[13] T. Liu,[13] M. Saulnier,[13] R. Wilson,[13] H. Yamamoto,[13] T. Bergfeld,[14] B.I. Eisenstein,[14] G. Gollin,[14] B. Ong,[14] M. Palmer,[14] M. Selen,[14] J. J. Thaler,[14] K.W. Edwards,[15] M. Ogg,[15] A. Bellerive,[16] D.I. Britton,[16] E.R.F. Hyatt,[16] D.B. MacFarlane,[16] P.M. Patel,[16] B. Spaan,[16] A.J. Sadoff,[17] R. Ammar,[18] P. Baringer,[18] A. Bean,[18] D. Besson,[18] D. Coppage,[18] N. Copty,[18] R. Davis,[18] N. Hancock,[18] M. Kelly,[18] S. Kotov,[18] I. Kravchenko,[18] N. Kwak,[18] H. Lam,[18] Y. Kubota,[19] M. Lattery,[19] M. Momayezi,[19] J.K. Nelson,[19] S. Patton,[19] R. Poling,[19] V. Savinov,[19] S. Schrenk,[19] R. Wang,[19] M.S. Alam,[20] I.J. Kim,[20] Z. Ling,[20] A.H. Mahmood,[20] J.J. O'Neill,[20] H. Severini,[20] C.R. Sun,[20] F. Wappler,[20] G. Crawford,[21] C. M. Daubenmier,[21] R. Fulton,[21] D. Fujino,[21] K.K. Gan,[21] K. Honscheid,[21] H. Kagan,[21] R. Kass,[21] J. Lee,[21] R. Malchow,[21] M. Sung,[21] C. White,[21] M.M. Zoeller,[21] F. Butler,[22] X. Fu,[22] B. Nemati,[22] W.R. Ross,[22] P. Skubic,[22] and M. Wood[22]

(CLEO Collaboration)

[1] *Purdue University, West Lafayette, Indiana 47907*
[2] *University of Rochester, Rochester, New York 14627*
[3] *Southern Methodist University, Dallas, Texas 75275*
[4] *Syracuse University, Syracuse, New York 13244*
[5] *Vanderbilt University, Nashville, Tennessee 37235*
[6] *Virginia Polytechnic Institute and State University, Blacksburg, Virginia, 24061*
[7] *California Institute of Technology, Pasadena, California 91125*
[8] *University of California, San Diego, La Jolla, California 92093*
[9] *University of California, Santa Barbara, California 93106*
[10] *University of Colorado, Boulder, Colorado 80309-0390*
[11] *Cornell University, Ithaca, New York 14853*
[12] *University of Florida, Gainesville, Florida 32611*
[13] *Harvard University, Cambridge, Massachusetts 02138*
[14] *University of Illinois, Champaign-Urbana, Illinois, 61801*
[15] *Carleton University, Ottawa, Ontario K1S 5B6 and the Institute of Particle Physics, Canada*
[16] *McGill University, Montréal, Québec H3A 2T8 and the Institute of Particle Physics, Canada*
[17] *Ithaca College, Ithaca, New York 14850*
[18] *University of Kansas, Lawrence, Kansas 66045*
[19] *University of Minnesota, Minneapolis, Minnesota 55455*
[20] *State University of New York at Albany, Albany, New York 12222*
[21] *Ohio State University, Columbus, Ohio, 43210*
[22] *University of Oklahoma, Norman, Oklahoma 73019*

## Abstract

We have observed four new decay modes of the charmed baryon $\Lambda_c^+$ using data collected with the CLEO II detector. Three decay modes, $\Lambda_c^+ \to p\bar{K}^0\eta$, $\Lambda\eta\pi^+$, and $\Sigma^+\eta$, are first observations of final states with an $\eta$ meson, while the fourth mode, $\Lambda_c^+ \to \Lambda\bar{K}^0K^+$, requires an $s\bar{s}$ quark pair to be popped out of the vacuum. The branching ratios relative to $\Lambda_c^+ \to pK^-\pi^+$ are measured to be $0.25\pm0.05\pm0.04$, $0.36\pm0.06\pm0.05$, $0.10\pm0.03\pm0.02$, and $0.11\pm0.02\pm0.02$, respectively.

*Permanent address: University of Hawaii at Manoa

## I. INTRODUCTION

In the past year, CLEO has measured the exclusive decays of the $\Lambda_c^+$ into $\Lambda(n\pi)^+$, $\Sigma^0(n\pi)^+$, $\Sigma^+(n\pi)^0$, $pK^-(n\pi)^+$, and $pK_s^0(n\pi)^0$, where $n \leq 3$ and includes up to one $\pi^0$ [1–4]. In addition, CLEO has observed decays that are expected to occur solely through the W-exchange diagram, namely, $\Lambda_c^+ \to \Sigma^+K^+K^-$, $\Xi^0K^+$, and $\Xi^-K^+\pi^+$ [5]. Figure 1 displays these branching fractions relative to the normalizing decay mode $\Lambda_c^+ \to pK^-\pi^+$. Many of these modes were first observations, especially modes that contain neutral particles, for which the CLEO detector is highly efficient. Using the PDG value of $\mathcal{B}(\Lambda_c^+ \to pK^-\pi^+) = (3.2 \pm 0.7)\%$ [6], only $\sim$25% of the $\Lambda_c^+$ hadronic decay modes have been observed. Missing from this catalog of $\Lambda_c^+$ decays are higher multiplicity modes, especially those that have multiple $\pi^0$'s. Also missing are decay modes that have $\Sigma^-$ hyperons or neutrons in the final state since these decays are difficult to observe. There are clearly a substantial number of $\Lambda_c^+$ decay modes which remain to be discovered.

This paper presents new results on four $\Lambda_c^+$ decay modes. These include the first observation of three $\Lambda_c^+$ decay modes with $\eta$'s in the final state, namely $\Lambda_c^+ \to pK_s^0\eta$, $\Lambda\eta\pi^+$, and $\Sigma^+\eta$. The fourth mode is $\Lambda_c^+ \to \Lambda K_s^0K^+$, which involves popping an $s\bar{s}$ quark pair.

## II. PARTICLE IDENTIFICATION

The data were collected with the CLEO II detector at the Cornell $e^+e^-$ storage ring CESR, which operated on, and just below, the $\Upsilon(4S)$ resonance. The CLEO II detector [7] is a large solenoidal detector with 67 tracking layers and a CsI electromagnetic calorimeter that provides efficient $\pi^0$ and $\eta$ reconstruction. We have used a total integrated luminosity of 3.25 fb$^{-1}$, which corresponds to roughly 4 million $c\bar{c}$ events.

Most of the $\Lambda_c^+$ decay modes discussed in this report have an $\eta$ meson in the final state. The $\eta$ candidates are selected through their decay $\eta \to \gamma\gamma$ from pairs of well-defined showers in the CsI calorimeter. To reduce combinatorics from soft photons, we require $E_\gamma > 0.15$ GeV for each photon candidate and $P_\eta > 0.5$ GeV/c. The photon candidates must not be associated with charged tracks and must have lateral shower shapes consistent with that expected for true photons [8]. At least one of the photon candidates must lie in the good barrel region ($|\cos\theta| < 0.71$). Finally, photons are vetoed if they can be paired with a second photon such that the $\gamma\gamma$ pair has an invariant mass within $2.5\sigma$ of the $\pi^0$ mass and a momentum greater than 1.0 GeV/c. From Monte Carlo simulations, the efficiency for detecting $\eta$'s with $P_\eta > 0.5$ GeV/c is about 30%. Figure 2 shows the $M_{\gamma\gamma}$ distribution after all the cuts have been applied. The $\eta$ signal has a width of approximately 14 MeV/c$^2$ and a mean consistent with the true $\eta$ mass. Since the signal shape is asymmetric, we select $\eta$ candidates in the mass range $M_{\gamma\gamma} = 515 - 575$ MeV/c$^2$. Finally, we kinematically fit the photon momenta to the nominal $\eta$ mass in order to improve the $\eta$ momentum estimate.

Protons, kaons, and pions are identified using dE/dx and time-of-flight information, when available. For protons we require PRLEV>0.1, where PRLEV is the relative probability that the track is a proton

$$\mathrm{PRLEV} = \frac{\mathcal{P}(p)}{\mathcal{P}(p) + \mathcal{P}(K) + \mathcal{P}(\pi)} \tag{1}$$

and $\mathcal{P}$ is the $\chi^2$ probability that the track satisfies a given hypothesis. Strong proton identification (PRLEV>0.9) is employed for modes with high background levels, *e.g.* $\Lambda_c^+ \to pK_s^0\eta$. A track is considered as a kaon candidate if the probability $\mathcal{P}(K)$ is at least 1%. Finally, we require that a track have a dE/dx measurement consistent with the pion hypothesis (within $\pm3\sigma$) to be identified as a pion. We use a pure sample of $\Lambda \to p\pi^-$, $D^0 \to K^-\pi^+$ from $D^{*+}$'s, and $K_s^0 \to \pi^+\pi^-$ to measure the particle identification efficiency for protons, kaons, and pions, respectively. The efficiency for weak and strong proton identification as a function of proton momentum is shown in Figure 3. Weak proton identification is 95% efficient for momenta below 0.5 GeV/c and falls smoothly to 85% at 2.5 GeV/c. Strong proton identification improves the signal to noise, but quickly becomes inefficient above 1.5 GeV/c. Charged pions and kaons are identified with an efficiency of $\sim$ 99% and $\sim$ 96%, respectively.

$K_s^0$ and $\Lambda$ candidates are selected through their decays $K_s^0 \to \pi^+\pi^-$ and $\Lambda \to p\pi^-$ by reconstructing a secondary decay vertex. Detached vertices are reconstructed from the intersection of two oppositely charged tracks in the $r-\phi$ plane. We cut on the impact parameter of the daughter tracks, and require that the decay length be at least 1 mm from the interaction point in the $r-\phi$ plane. We also cut on the $\chi^2$ of the reconstructed decay vertex, which requires both the miss distance in $\hat{z}$ between the two tracks at the estimated decay vertex and the impact parameter of the $K_s^0$ or $\Lambda$ to be small. The proton for the $\Lambda$ candidate must satisfy PRLEV>0.1. Finally, the invariant masses of the $K_s^0$ and $\Lambda$ candidates must be within 15 MeV/c$^2$ and 5 MeV/c$^2$ of their nominal values, respectively.

The $\Sigma^+$ particle is identified through its decay into $p\pi^0$ [3]. The $\Sigma^+$ lifetime is long ($c\tau$ = 2.4cm), hence protons from $\Sigma^+$ decays have large impact parameters. The proton candidate must have an impact parameter greater than 0.6 mm, a momentum greater than 0.5 GeV/c, and PRLEV> 0.1. The $\pi^0$ candidate is chosen from pairs of shower clusters not matched to charged tracks. The photons must have $E_\gamma > 30$ MeV and a lateral shower shape consistent with that of a true photon. At least one of the photons must lie in the good barrel region, and $P_{\pi^0}$ must be greater than 0.2 GeV/c. The $\pi^0$ and $\Sigma^+$ invariant masses are initially computed assuming the particles originate from the primary vertex. These mass measurements are refined by recomputing them at the location of the $\Sigma^+$ decay vertex. The procedure is as follows: the $\Sigma^+$ candidate is assumed to originate from the primary vertex. We then estimate the $\Sigma^+$ decay vertex to be the point along the proton trajectory where the proton and $\Sigma^+$ intersect in the $r-\phi$ plane. We require that the miss distance between the proton and the $\Sigma^+$ along the beam axis ($\hat{z}$) be less than 10 mm, the recomputed $\pi^0$ mass be 120–150 MeV/c$^2$, and the decay vertex lie in the direction of the $\Sigma^+$ momentum. The $M_{p\pi^0}$ spectrum for $P_{p\pi^0} > 1$ GeV/c is shown in Figure 4. We observe $13100 \pm 300$ $\Sigma^+$ hyperons with a width of $5.0 \pm 0.1$ MeV/c$^2$ and a mass of $1188.8 \pm 0.1$ MeV/c$^2$, consistent with the nominal $\Sigma^+$ mass. Without the vertex correction, the $M_{p\pi^0}$ signal would be considerably broader. The efficiency for reconstructing $\Sigma^+ \to p\pi^0$ decays in this momentum range is about 15%. We select $\Sigma^+$ candidates that lie within 15 MeV/c$^2$ of the nominal $\Sigma^+$ mass.

Finally, charged tracks that do not arise from long-lived particles ($\Lambda$, $K_s^0$, and $\Sigma^+$) must have a distance of closest approach in the $r-\phi$ plane of less than 5 mm to the interaction point, and be within 5 cm in $\hat{z}$.

## III. $\Lambda_c^+ \to pK_s^0\eta$

The decay mode $\Lambda_c^+ \to pK_s^0\eta$ may occur via an internal spectator diagram or a W-exchange diagram; the external spectator diagram cannot contribute. The selection of protons, $K_s^0$'s, and $\eta$'s has been described in the previous section. Charm baryons from $e^+e^-$ interactions are produced with a hard momentum spectrum, so we can reduce the combinatoric background by requiring $x_p(\Lambda_c^+) > 0.5$, where $x_p(\Lambda_c^+) = P_{\Lambda_c^+}/\sqrt{E_{beam}^2 - M_{\Lambda_c^+}^2}$ is the scaled momentum of the $\Lambda_c^+$. The $x_p$ cut also eliminates $\Lambda_c^+$ baryons that arise from $B$ meson decays. We further require that the Fox-Wolfram event shape parameter $R_2$ [9] be greater than 0.2, so that the background contribution in the $\Lambda_c^+$ signal region due to $B\bar{B}$ production is reduced. The $R_2$ cut is used for all $\Lambda_c^+$ decay modes.

In addition, we impose strong particle ID on the proton, and require the three daughter particles to be in the same jet hemisphere by demanding that the daughter tracks lie within 90 degrees of the $\Lambda_c^+$ momentum vector. The invariant mass distribution for $\Lambda_c^+ \to pK_s^0\eta$ in the data is shown in Figure 5. We fit the signal to a Gaussian and the background to a 3rd order Chebyshev polynomial. The Gaussian width is fixed to the Monte Carlo prediction of 6.6 MeV/c$^2$, while the mean is allowed to float. We observe $53 \pm 10$ $pK_s^0\eta$ events at a mass of $2287 \pm 2$ MeV/c$^2$ (statistical error only), consistent with the nominal $\Lambda_c^+$ mass. Backgrounds from misidentified $D^+$ and $D_s^+$ decays to $K_s^0\eta\pi^+$ in which the pion has been misidentified as a proton are not observed.

Since we do not know the overall $\Lambda_c^+$ cross section, we convert our observation into a branching fraction relative to the well measured decay $\Lambda_c^+ \to pK^-\pi^+$. We apply the same proton identification (PRLEV$> 0.9$) and $\Lambda_c^+$ momentum cut ($x_p > 0.5$) to the $\Lambda_c^+ \to pK^-\pi^+$ sample in order to reduce the systematic errors associated with these cuts. In addition, the daughter tracks are required to lie in the same jet hemisphere. A fit to the $pK^-\pi^+$ invariant mass distribution using the Monte Carlo predicted width yields $4910 \pm 134$ events. For $x_p > 0.5$ the Monte Carlo-based efficiencies to reconstruct the decay modes $\Lambda_c^+ \to pK_s^0\eta$ and $\Lambda_c^+ \to pK^-\pi^+$ are $(7.3 \pm 0.2)\%$ and $(22.3 \pm 0.3)\%$, respectively. After taking into account the $\bar{K}^0$ and $\eta$ branching fractions to the final states we observe them in, the ratio of branching fractions is

$$\frac{\mathcal{B}(\Lambda_c^+ \to p\bar{K}^0\eta)}{\mathcal{B}(\Lambda_c^+ \to pK^-\pi^+)} = 0.25 \pm 0.05 \pm 0.04 \qquad (2)$$

where the first error is statistical and the second is systematic (to be discussed later). This decay rate is about 2.5 times smaller than the related mode in which the $\eta$ is replaced by a $\pi^0$, which CLEO [4] measures to be $\mathcal{B}(\Lambda_c^+ \to p\bar{K}^0\pi^0)/\mathcal{B}(\Lambda_c^+ \to pK^-\pi^+) = 0.63 \pm 0.13$. This is consistent with the light quark content of the $\eta$ being roughly one-third that of the $\pi^0$.

## IV. $\Lambda_c^+ \to \Lambda\eta\pi^+$

The decay $\Lambda_c^+ \to \Lambda\eta\pi^+$ can occur through three diagrams: external spectator, internal spectator and W-exchange. To reduce the combinatoric background, we require the $\Lambda$, $\pi^+$, and $\eta$ to be in the same jet hemisphere. We also place a higher momentum cut on the $\Lambda_c^+$, namely $x_p > 0.6$, as the backgrounds are higher in this decay mode. The invariant mass distribution for $\Lambda\eta\pi^+$ is shown in Figure 6. The signal is fit to a Gaussian with the width fixed to the Monte Carlo expectation of $\sigma_{\Lambda_c^+} = 8.6$ MeV/c$^2$, and the background is parametrized by a 2nd order Chebyshev polynomial. We observe $109 \pm 16$ events at a mass of $2289 \pm 2$ MeV/c$^2$.

Because we impose only weak particle ID on the proton, about 3% of the $\Lambda$ candidates are actually $K_s^0$ particles. Backgrounds may arise from $D^+$ and $D_s^+$ decays to $K_s^0\eta\pi^+$, where the $K_s^0$ has been misidentified as a $\Lambda$. Examination of the $K_s^0\eta\pi^+$ and $K_s^0$ invariant mass spectra for combinations passing the selection criteria show no evidence for such backgrounds.

Applying the same proton identification and $x_p$ cut to the $pK^-\pi^+$ sample yields $6282\pm243$ events. For $x_p > 0.6$ the efficiency to reconstruct the $\Lambda_c^+ \to \Lambda\eta\pi^+$ and $\Lambda_c^+ \to pK^-\pi^+$ decays modes are $(8.5 \pm 0.3)\%$ and $(44.2 \pm 0.5)\%$, respectively. The $pK^-\pi^+$ efficiency is higher here than in the previous case due to the looser proton identification requirement. After accounting for the $\Lambda$ and $\eta$ branching fractions, the ratio of branching fractions is

$$\frac{\mathcal{B}(\Lambda_c^+ \to \Lambda\eta\pi^+)}{\mathcal{B}(\Lambda_c^+ \to pK^-\pi^+)} = 0.36 \pm 0.06 \pm 0.05 \tag{3}$$

This again is about a factor of two smaller than the related decay mode $\Lambda_c^+ \to \Lambda\pi^+\pi^0$ in which the $\eta$ has been replaced by a $\pi^0$. For this mode, CLEO [2] has measured $\mathcal{B}(\Lambda_c^+ \to \Lambda\pi^+\pi^0)/\mathcal{B}(\Lambda_c^+ \to pK^-\pi^+) = 0.73 \pm 0.09 \pm 0.16$.

We have also studied the resonant substructure for the decay $\Lambda_c^+ \to \Lambda\eta\pi^+$. In addition to non-resonant phase space decays, two decay chains are possible: $\Lambda_c^+ \to \Sigma^{*+}(1385)\eta$ with $\Sigma^{*+}(1385) \to \Lambda\pi^+$, and $\Lambda_c^+ \to \Lambda a_0^+(980)$ with $a_0^+(980) \to \eta\pi^+$. Figure 7 shows the Dalitz plot of $M^2_{\Lambda\pi^+}$ versus $M^2_{\eta\pi^+}$ for $\Lambda\eta\pi^+$ candidates within $\pm2\sigma$ of the $\Lambda_c^+$ mass. In order to increase the $\Lambda_c^+$ signal-to-background ratio, we have tightened the $\pi^0$ veto for $\eta$ candidates by eliminating photons that are consistent with arising from a $\pi^0$ of any momentum. Both the $\Sigma^{*+}(1385)$ and $a_0^+(980)$ are broad resonances [10]. Evidence for $\Sigma^{*+}(1385)$ would appear as a band at $M^2_{\Lambda\pi^+} \approx 1.9$ (GeV/c$^2$)$^2$. Similarly, a band at $M^2_{\eta\pi^+} \approx 0.96$ (GeV/c$^2$)$^2$ would indicate presence of the scalar $a_0(980)$ resonance. In Figure 8(a) we have projected the Dalitz plot onto the $M^2_{\Lambda\pi^+}$ axis and performed a $\Lambda_c^+$ sideband subtraction. A fit to the $M^2_{\Lambda\pi^+}$ distributions using the Monte Carlo distributions for $M^2_{\Lambda\pi^+}$ from $\Sigma^{*+}(1385)\eta$ resonant and phase space decays suggests that $(37 \pm 14)\%$ (statistical errors only) of the $\Lambda\eta\pi^+$ signal proceeds via the $\Sigma^{*+}(1385)$ resonance. Here, we have assumed that the different amplitudes due to resonant substructure add incoherently. Likewise, a projection onto the $M^2_{\eta\pi^+}$ axis suggests that $(39 \pm 14)\%$ of the $\Lambda\eta\pi^+$ signal proceeds through the $a_0(980)$ resonance, seen in Figure 8(b). However, an upper limit of 33% (90% CL) can also be placed on this process because no significant $a_0^+(980) \to K_s^0K^+$ resonant substructure is evident in the related decay mode $\Lambda_c^+ \to \Lambda K_s^0K^+$, as is discussed in Section VI. Here, we have assumed that $\mathcal{B}(a_0(980) \to \bar{K}^0K^+)/\mathcal{B}(a_0(980) \to \eta\pi^+) = 0.25 \pm 0.05$ [11].

## V. $\Lambda_c^+ \to \Sigma^+\eta$

The two-body decay $\Lambda_c^+ \to \Sigma^+\eta$ is particularly significant since this decay is not expected to arise via an external spectator diagram. Identification of the $\Sigma^+$ and $\eta$ candidates is described in Section II. Because four photons exist in the final state, the combinatoric

TABLE I. Comparison of experimental branching fractions to theoretical predictions for the two-body decays $\Lambda_c^+ \to \Sigma^+\pi^0$ and $\Sigma^+\eta$ relative to $\mathcal{B}(\Lambda_c^+ \to pK^-\pi^+)$ .

| | $\mathcal{B}(\Lambda_c^+ \to \Sigma^+\pi^0)/B(pK^-\pi^+)$ | $\mathcal{B}(\Lambda_c^+ \to \Sigma^+\eta)/B(pK^-\pi^+)$ |
|---|---|---|
| CLEO | $0.20 \pm 0.03 \pm 0.03$ | $0.10 \pm 0.03 \pm 0.02$ |
| Körner and Krämer [12] | 0.10 | 0.05 |
| Zenczykowski [13] | 0.13 | 0.08 |

background can be severe. Photons from the $\pi^0$ tend to be extremely soft, and so the inclusion of random soft photons can still produce $\pi^0$, $\Sigma^+$, and $\Lambda_c^+$ candidates with invariant masses satisfying the selection criteria. As described in the particle ID section for $\Sigma^+$, we reduce the combinatoric background by requiring the $\pi^0$ to have a momentum $P_{\pi^0} > 0.2$ GeV/c. We also demand that the $\eta$, $\Sigma^+$, and $\Sigma^+\eta$ candidates have high momenta: $P_\eta > 0.8$ GeV/c, $P_{\Sigma^+} > 1.0$ GeV/c, and $x_p(\Lambda_c^+) > 0.6$, respectively. Figure 9 shows the $\Sigma^+\eta$ invariant mass distribution after applying all the selection cuts. We fit this distribution to a Gaussian whose width is fixed to the Monte Carlo prediction of $\sigma_{\Lambda_c^+} = 20$ MeV/c$^2$, and a quadratic background. We observe preliminary evidence for $\Lambda_c^+ \to \Sigma^+\eta$ consisting of $16.6 \pm 5.2$ events at a mass of $2285 \pm 5$ MeV/c$^2$.

Due to the soft photon background, about 12% of the time events in the data are multiply counted in the $\Sigma^+\eta$ mass distribution. The multiple entries are distributed uniformly over the mass range 2.0–2.6 GeV/c$^2$. The Monte Carlo models this effect well, and so we increase the statistical error from the fit by 6%.

Applying the same proton identification and $x_p$ requirement on the $pK^-\pi^+$ sample yields $6282 \pm 243$ events. For $x_p > 0.6$ the efficiency to reconstruct the $\Lambda_c^+ \to \Sigma^+\eta$ and $\Lambda_c^+ \to pK^-\pi^+$ modes are $(5.2\pm0.2)$% and $(44.2\pm0.5)$%, respectively. Accounting for the branching fractions of $\Sigma^+$ and $\eta$, we obtain the ratio of branching fractions to be

$$\frac{\mathcal{B}(\Lambda_c^+ \to \Sigma^+\eta)}{\mathcal{B}(\Lambda_c^+ \to pK^-\pi^+)} = 0.10 \pm 0.03 \pm 0.02 \tag{4}$$

This decay rate is about half that of the related two-body decay mode, $\Lambda_c^+ \to \Sigma^+\pi^0$, which has been measured by CLEO [3] to be $\mathcal{B}(\Lambda_c^+ \to \Sigma^+\pi^0)/\mathcal{B}(\Lambda_c^+ \to pK^-\pi^+) = 0.20\pm0.03\pm0.03$.

Körner and Krämer [12] and Zenczykowski [13] have made theoretical predictions for $\Lambda_c^+$ decays into two-body final states with $\Sigma^+$ hyperons. We have converted their decay rates into relative branching fractions using the PDG values for the $\Lambda_c^+$ lifetime and $\mathcal{B}(\Lambda_c^+ \to pK^-\pi^+)$ [6]. The theoretical estimates, shown in Table I, agree with our results within a factor of two. Moreover, both groups predict that the ratio $\mathcal{B}(\Sigma^+\eta)/\mathcal{B}(\Sigma^+\pi^0)$ is 0.5–0.6, in agreement with our measurement.

## VI. $\Lambda_c^+ \to \Lambda K_s^0 K^+$

The decay $\Lambda_c^+ \to \Lambda K_s^0 K^+$ is analogous to the decay $\Lambda_c^+ \to \Lambda\pi^+\pi^0$ except that an $s\bar{s}$ quark pair must be popped out of the vacuum. We extract this decay mode by finding the $\Lambda$, $K_s^0$,

TABLE II. Summary of results on new $\Lambda_c^+$ decay modes. The efficiencies do not include branching fractions to the observed final states.

| $\Lambda_c^+$ decay mode | Number of events | $x_p$ cut | Efficiency (%) | $\mathcal{B}/\mathcal{B}(\Lambda_c^+ \to pK^-\pi^+)$ |
|---|---|---|---|---|
| $p\bar{K}^0\eta$ | $53 \pm 10$ | 0.5 | 7.3 | $0.25 \pm 0.05 \pm 0.04$ |
| $\Lambda\eta\pi^+$ | $109 \pm 16$ | 0.6 | 8.5 | $0.36 \pm 0.06 \pm 0.05$ |
| $\Sigma^+\eta$ | $25 \pm 7$ | 0.6 | 5.2 | $0.10 \pm 0.03 \pm 0.02$ |
| $\Lambda\bar{K}^0K^+$ | $46 \pm 8$ | 0.4 | 7.9 | $0.11 \pm 0.02 \pm 0.02$ |

and $K^+$ as described in Section II, and by requiring the three particles to be in the same jet hemisphere. Since the phase space for this decay is small and the $K_s^0$ and $\Lambda$ signals are relatively clean, we can relax the $\Lambda_c^+$ momentum cut to $x_p > 0.4$ without greatly increasing the combinatoric background. Figure 10 shows the $\Lambda K_s^0 K^+$ invariant mass distribution for the data, where we observe a $\Lambda_c^+$ signal of $46 \pm 8$ events at a mass of $M_{\Lambda_c^+} = 2286 \pm 1$ MeV/c$^2$. Here, we have fixed the Gaussian width to the Monte Carlo expectation $\sigma_{\Lambda_c^+} = 4.1$ MeV/c$^2$ and assumed a linear background.

We have checked that the decay $D^+ \to K_s^0 K_s^0 K^+$ in which a $K_s^0$ is misidentified as a $\Lambda$, or the doubly misidentified decay $D_s^+ \to K_s^0 K_s^0 \pi^+$ does not contribute to the $\Lambda_c^+$ signal region. We also do not observe any resonant substructure in the decay $\Lambda_c^+ \to \Lambda K_s^0 K^+$. In particular, the fraction of $K_s^0 K^+$ from the $a_0(980)$ resonance is less than 30% at the 90% confidence level.

The $\Lambda_c^+ \to pK^-\pi^+$ sample yields $9288 \pm 314$ events, after applying the same proton and kaon identification and $x_p$ cut. For $x_p > 0.4$ the efficiency to reconstruct the $\Lambda_c^+ \to \Lambda K_s^0 K^+$ and $\Lambda_c^+ \to pK^-\pi^+$ decay modes are $(7.9 \pm 0.2)$% and $(38.1 \pm 0.4)$%, respectively. After accounting for the $\Lambda$ and $\bar{K}^0$ branching fractions, we obtain the ratio of branching fractions to be

$$\frac{\mathcal{B}(\Lambda_c^+ \to \Lambda\bar{K}^0K^+)}{\mathcal{B}(\Lambda_c^+ \to pK^-\pi^+)} = 0.11 \pm 0.02 \pm 0.02 \tag{5}$$

This is roughly 7 times smaller than the related decay mode without $s\bar{s}$ popping, $\Lambda_c^+ \to \Lambda\pi^+\pi^0$, which CLEO [2] measures to be $\mathcal{B}(\Lambda_c^+ \to \Lambda\pi^+\pi^0)/\mathcal{B}(\Lambda_c^+ \to pK^-\pi^+) = 0.73 \pm 0.09 \pm 0.16$. A summary of all the $\Lambda_c^+$ decay modes studied in this analysis is presented in Table II.

## VII. SYSTEMATICS

The systematic errors associated with the measured branching fractions of the new $\Lambda_c^+$ decay modes are listed in Table III. The systematic errors due to uncertainties in the proton identification and the $\Lambda_c^+$ momentum spectrum are greatly reduced by normalizing the branching fraction to the reference decay mode $\Lambda_c^+ \to pK^-\pi^+$. Weak proton ID has a relatively flat efficiency over the entire proton momentum range, so uncertainties in the absolute efficiency cancel in the ratio. We are more sensitive to systematic uncertainties when tagging protons using strong particle ID since the efficiency falls off rapidly beyond

TABLE III. Sources of systematic errors.

| Source | Fractional Error (%) | | | |
|---|---|---|---|---|
| | $pK_s^0\eta$ | $\Lambda\eta\pi^+$ | $\Sigma^+\eta$ | $\Lambda K_s^0 K^+$ |
| $K_s^0$, $\Lambda$, and $\Sigma^+$ finding | 10 | 10 | 10 | 14 |
| $\eta$ and $\pi^0$ finding | 5 | 5 | 7 | — |
| Tracking efficiency | — | — | 4 | 4 |
| Proton and kaon identification | 8 | 2 | 2 | — |
| $pK^-\pi^+$ substructure | 7 | 2 | 2 | 5 |
| $\Lambda_c^+$ substructure | — | 6 | — | — |
| Uncertainties in $\sigma_{\Lambda_c^+}$ | 5 | 5 | 5 | 5 |
| Monte Carlo statistics | 3 | 3 | 3 | 3 |
| TOTAL | 16 | 14 | 14 | 16 |

TABLE IV. Comparison of relative $\Lambda_c^+$ branching fractions computed from high and low $x_p$ regions. The errors are statistical only.

| $x_p$ range | $\mathcal{B}(p\bar{K}^0\eta)/\mathcal{B}(pK^-\pi^+)$ | $\mathcal{B}(\Lambda\eta\pi^+)/\mathcal{B}(pK^-\pi^+)$ | $\mathcal{B}(\Lambda\bar{K}^0K^+)/\mathcal{B}(pK^-\pi^+)$ |
|---|---|---|---|
| 0.5–0.7 | $0.24 \pm 0.06$ | $0.33 \pm 0.07$ | $0.13 \pm 0.03$ |
| 0.7–1.0 | $0.28 \pm 0.08$ | $0.41 \pm 0.07$ | $0.07 \pm 0.03$ |

1.5 GeV/c and because the proton momentum spectrum differs between $pK_s^0\eta$ and $pK^-\pi^+$. We vary the position of the falloff by 50 MeV/c and see a 5% difference. In addition, the efficiency-corrected $\Lambda_c^+ \to pK^-\pi^+$ yields using weak and strong proton identification differ by 8%. We take this value as the total systematic error for applying strong proton ID.

The uncertainty in modeling the $\Lambda_c^+$ momentum spectrum can cause a systematic error in the ratio of branching fractions if the $\Lambda_c^+$ reconstruction efficiency differs as a function of $\Lambda_c^+$ momentum between the two decay modes. We have measured the $x_p$ distribution from our large sample of $\Lambda_c^+ \to pK^-\pi^+$ events and used this distribution to compute the average efficiency for each decay mode over the $\Lambda_c^+$ momentum range of interest. We assign this a systematic error of 1%. As a check, we divide the data into a high and low $x_p$ region and compute the relative branching fraction separately for both regions, as shown in Table IV. The relative branching fractions for $p\bar{K}^0\eta$ and $\Lambda\eta\pi^+$ are consistent, whereas the two for $\Lambda\bar{K}^0K^+$ differ by $1.6\sigma$.

We assign a systematic error of 2% for every charged track and 5% for every $\pi^0$ and $\eta$ in the final state. If we require that both photons from the $\eta$ come from the good barrel region, the efficiency for reconstructing $pK_s^0\eta$ and $\Lambda\eta\pi^+$ is reduced by 30%, but the difference in the efficiency-corrected yields are within errors. The systematic error for reconstructing $K_s^0$ and $\Lambda$ particles is studied by comparing the yields from the detached vertex reconstruction to the yields from the $\pi^+\pi^-$ and $p\pi^-$ invariant mass distributions where the masses are computed assuming the decay occurs at the origin. We perform this as a function of the $K_s^0$ and $\Lambda$ momentum. The Monte Carlo agrees with the data to within 10%. We calculated a

10% systematic error for reconstructing $\Sigma^+$ hyperons due to the cut on the proton impact parameter and by comparing the $\Sigma^+$ yields with and without using the estimated decay vertex.

The $\Lambda_c^+ \to pK^-\pi^+$ reconstruction efficiency is sensitive to whether the $\Lambda_c^+$ decays via phase space, $pK^{*0}$, or $\Delta^{++}K^-$. The variation depends on the selection criteria (2–7%) and is taken as a systematic error. Also, the efficiency for reconstructing $\Lambda_c^+ \to \Lambda\eta\pi^+$ depends on whether the decay proceeds according to phase space, $\Sigma^+(1385)\eta$, or $\Sigma^+ a_0(980)$. We assign a 6% systematic error due to the possible $\Lambda\eta\pi^+$ resonant substructure.

## VIII. CONCLUSIONS

We have observed four new decay modes of the charmed baryon $\Lambda_c^+$. Three decay modes, $\Lambda_c^+ \to p\bar{K}^0\eta$, $\Lambda\eta\pi^+$, and $\Sigma^+\eta$, contain an $\eta$ particle in the final state, while the fourth decay mode, $\Lambda_c^+ \to \Lambda\bar{K}^0K^+$, requires an $s\bar{s}$ quark pair to pop out of the vacuum. The branching fractions relative to the reference mode $\Lambda_c^+ \to pK^-\pi^+$ are measured to be $0.25 \pm 0.05 \pm 0.04$, $0.36 \pm 0.06 \pm 0.05$, $0.10 \pm 0.03 \pm 0.02$, and $0.11 \pm 0.02 \pm 0.02$, respectively. Altogether, the new modes account for roughly 3% of all $\Lambda_c^+$ decays. The $\Lambda\eta\pi^+$ decay mode appears to have a resonant substructure via $\Sigma^{*+}(1385)\eta$, but might also proceed through $\Sigma^+ a_0(980)$.

## ACKNOWLEDGEMENTS

We gratefully acknowledge the effort of the CESR staff in providing us with excellent luminosity and running conditions. This work was supported by the National Science Foundation, the U.S. Dept. of Energy, the Heisenberg Foundation, the SSC Fellowship program of TNRLC, Natural Sciences and Engineering Research Council of Canada, and the A.P. Sloan Foundation.

## REFERENCES


[1] Unless otherwise stated, the charge conjugate mode is always implied.

[2] CLEO Collaboration, P. Avery *et al.*, Phys. Lett. B **325**, 257(1994). No significant $\Lambda\rho^+$ or $\Sigma^*(1385)\pi$ resonant substructure was evident in the $\Lambda_c^+ \to \Lambda\pi^+\pi^0$ decay mode.

[3] CLEO Collaboration, Y. Kubota *et al.*, Phys. Rev. Lett. **71**, 3255(1993).

[4] CLEO Collaboration, D. Cinabro *et al.*, CLEO Conf 93-27, contrib. paper in Lepton Photon Conf. (1993).

[5] CLEO Collaboration, P. Avery *et al.*, Phys. Rev. Lett. **71**, 2391(1993).

[6] Particle Data Group, K. Hikasa *et al.*, Phys. Rev. D **45**, 1(1992).

[7] CLEO Collaboration, Y. Kubota *et al.*, Nucl. Inst. and Meth. **A320**, 66(1992).

[8] The shower shape is measured by the ratio of energy in the 9 crystals nearest the shower center to the energy in the 25 crystals nearest the shower center. For photons in our detector, this ratio peaks above 0.9.

[9] G.C. Fox and S. Wolfram, Phys. Rev. Lett. **41**, 1581(1978).

[10] The $\Sigma^*(1385)$ full width is $\Gamma = 36 \pm 1$ MeV/c$^2$ and the $a_0(980)$ full width is $\Gamma = 57 \pm 11$ MeV/c$^2$.

[11] The PDG reports that $\mathcal{B}(f_1(1285) \to \eta\pi\pi) = (50 \pm 5)\%$ and $\mathcal{B}(f_1(1285) \to K\bar{K}\pi) = (11.9 \pm 1.4)\%$. The WA76 Collaboration reports that both decays are dominated by $a_0(980)\pi$ with $a_0(980) \to \eta\pi$ and $K\bar{K}$. T.A. Armstrong *et al.*, Z. Phys. C **52**, 389(1991). T.A. Armstrong *et al.*, Phys. Lett. B **221**, 216(1989).

[12] J.G. Körner and M. Krämer, Z. Phys. C **55**, 659(1992).

[13] P. Zenczykowski, Phys. Rev. D **50**, 402(1994).

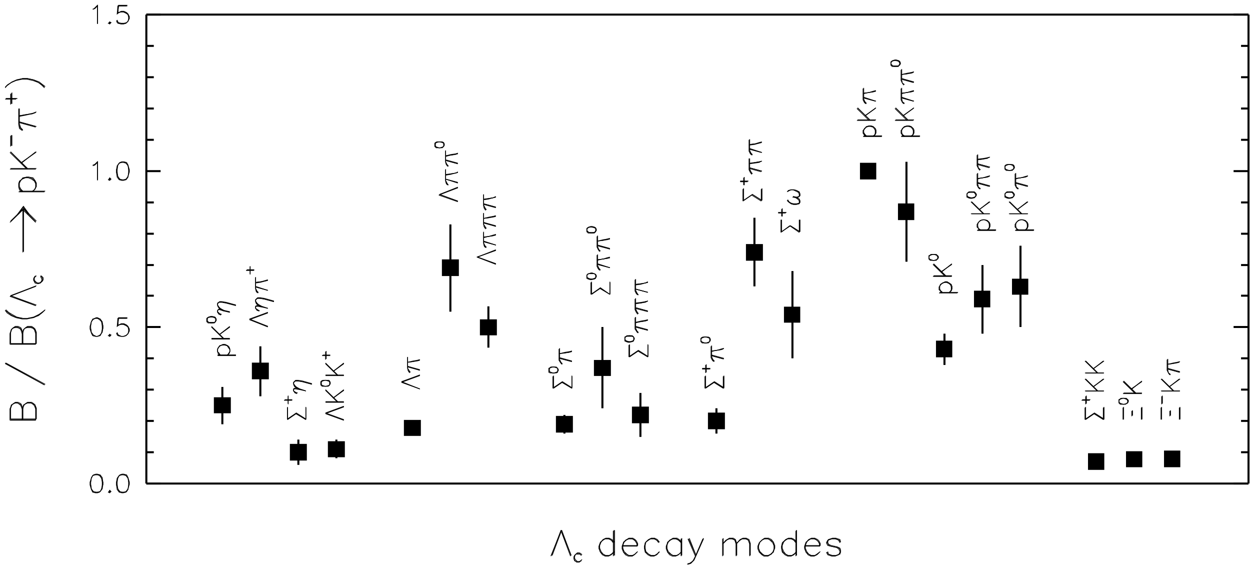


FIG. 1. Branching fractions of $\Lambda_c^+$ decays relative to the normalizing decay mode $\Lambda_c^+ \rightarrow pK^-\pi^+$ from recent CLEO measurements.

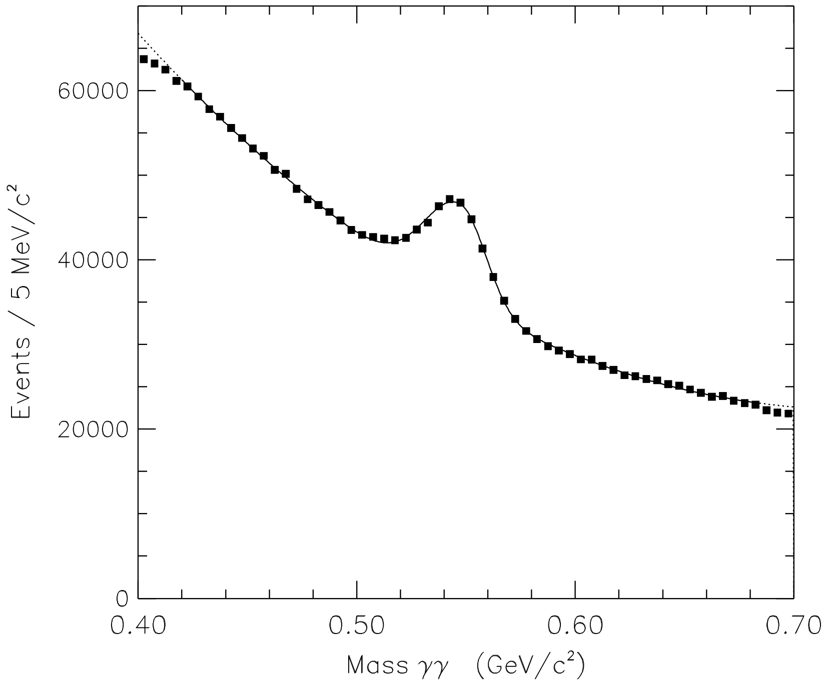


FIG. 2. Invariant mass distribution for $\eta \rightarrow \gamma\gamma$ with $P_\eta > 0.5$ GeV/c.

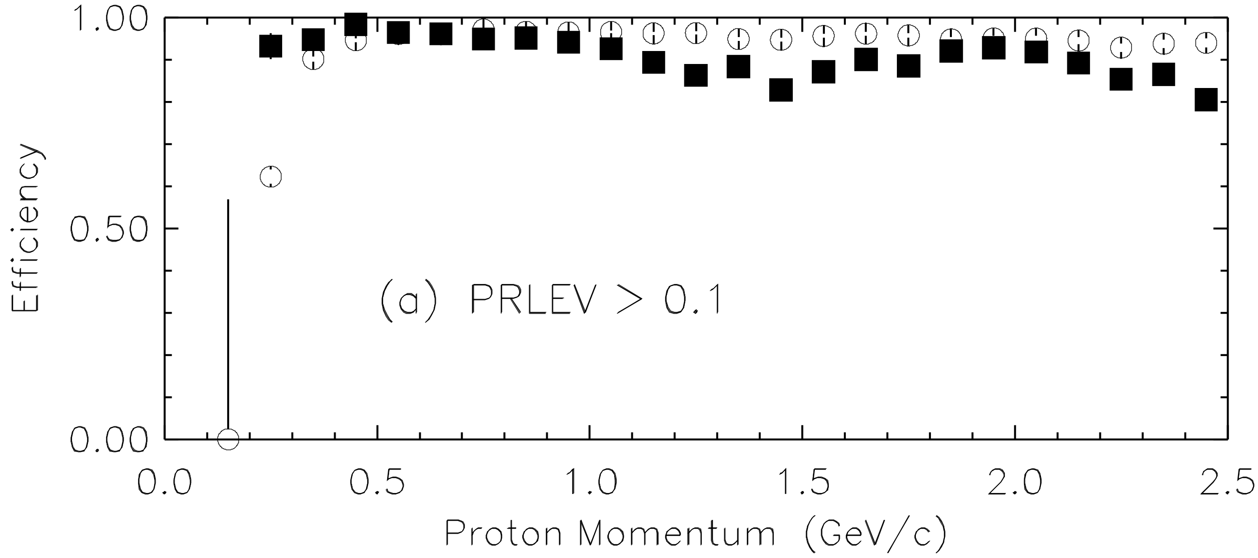


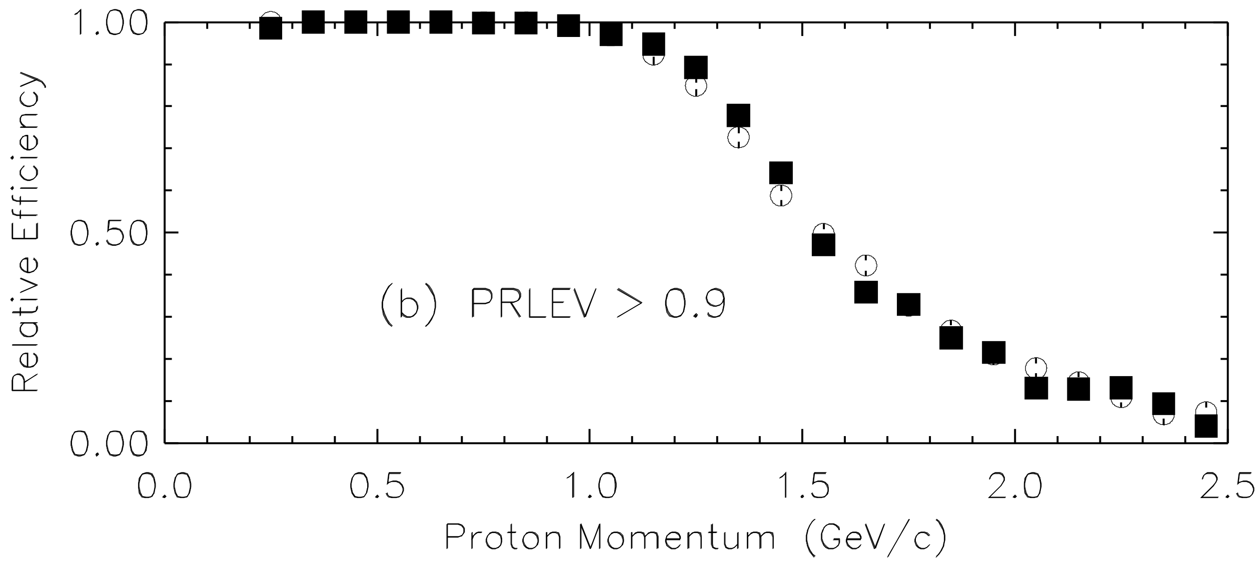


FIG. 3. Efficiency for selecting real protons with a weak or strong particle ID as a function of momentum for data (closed squares) and Monte Carlo (open circles). (a) PRLEV>0.1 efficiency, and (b) PRLEV>0.9 efficiency relative to the efficiency for protons to satisfy PRLEV>0.1.

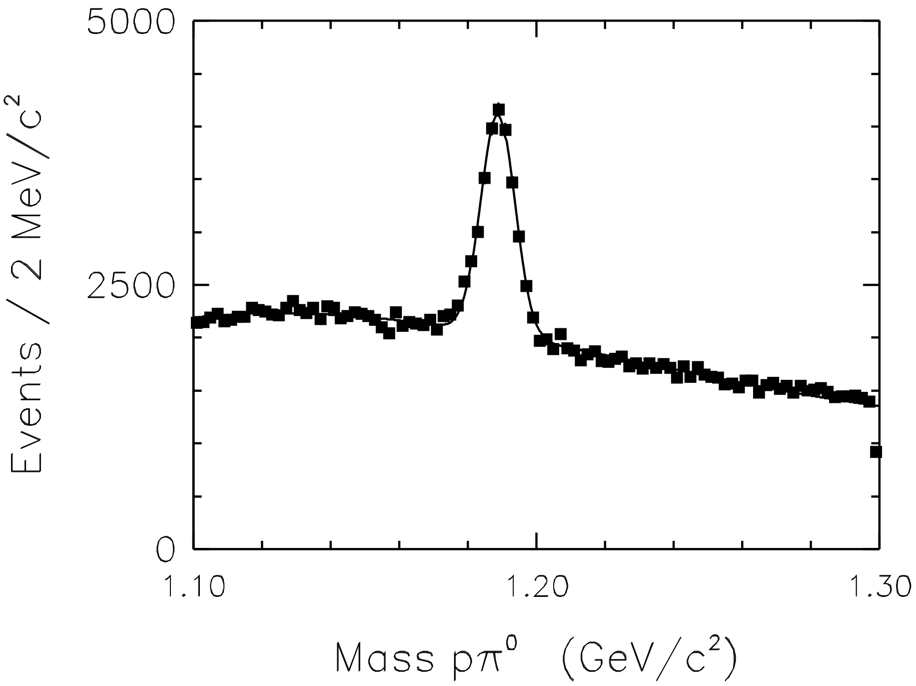


FIG. 4. Invariant mass distribution for $\Sigma^+ \rightarrow p\pi^0$ with $P_{\Sigma^+} > 1$ GeV/c.

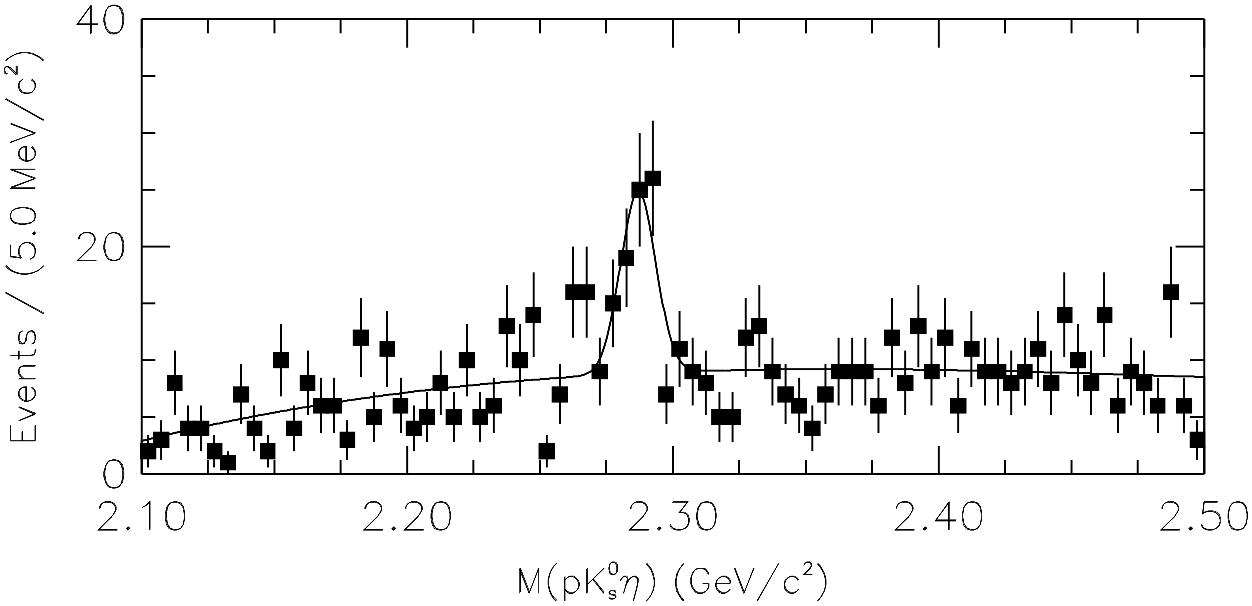


FIG. 5. Invariant mass distribution for $\Lambda_c^+ \rightarrow pK_s^0\eta$.

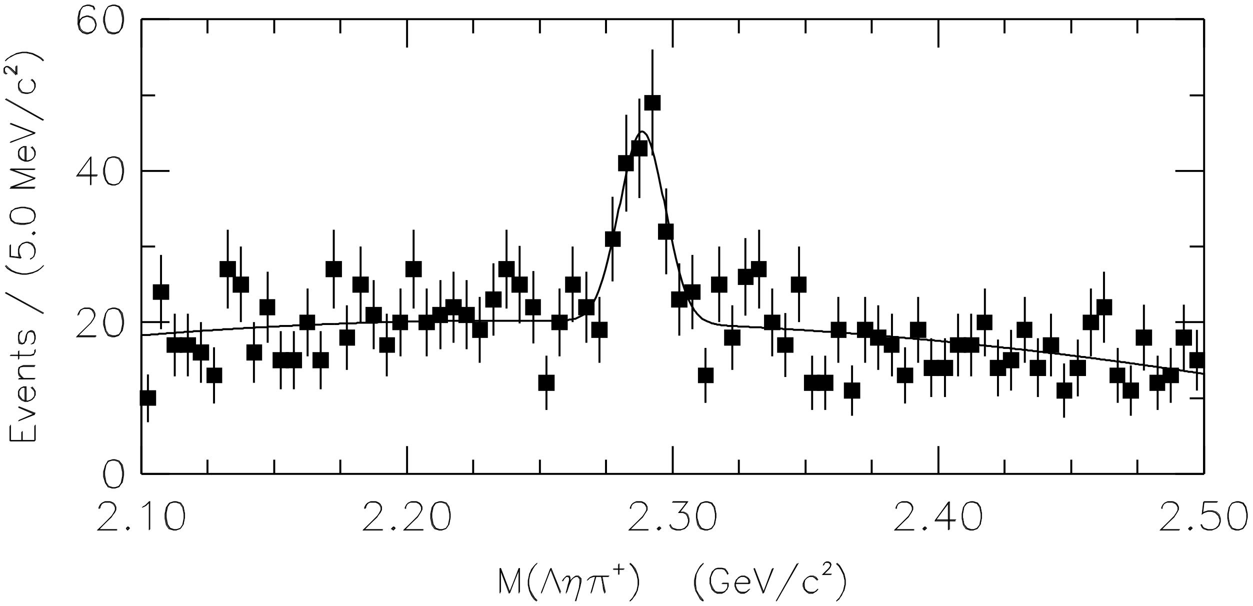


FIG. 6. Invariant mass distribution for $\Lambda_c^+ \to \Lambda\eta\pi^+$.

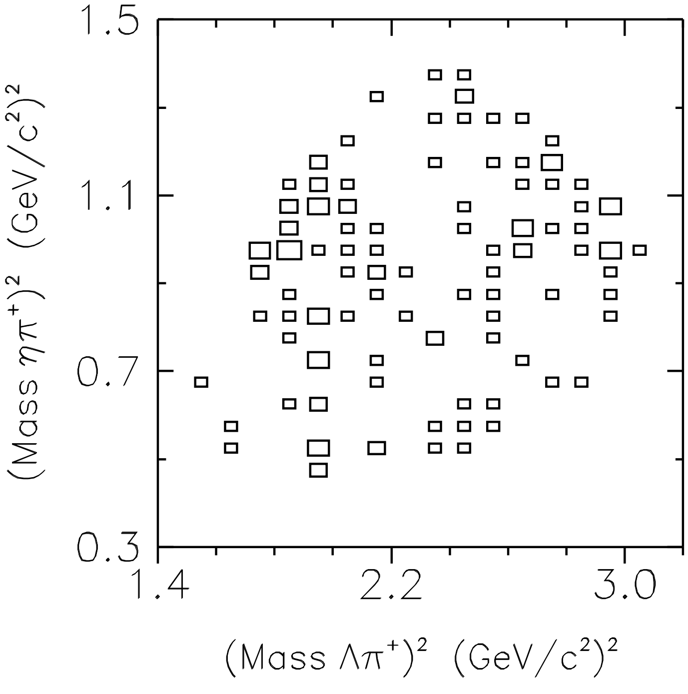


FIG. 7. Dalitz distribution for $\Lambda_c^+ \to \Lambda\eta\pi^+$: $M^2_{\Lambda\pi^+}$ versus $M^2_{\eta\pi^+}$

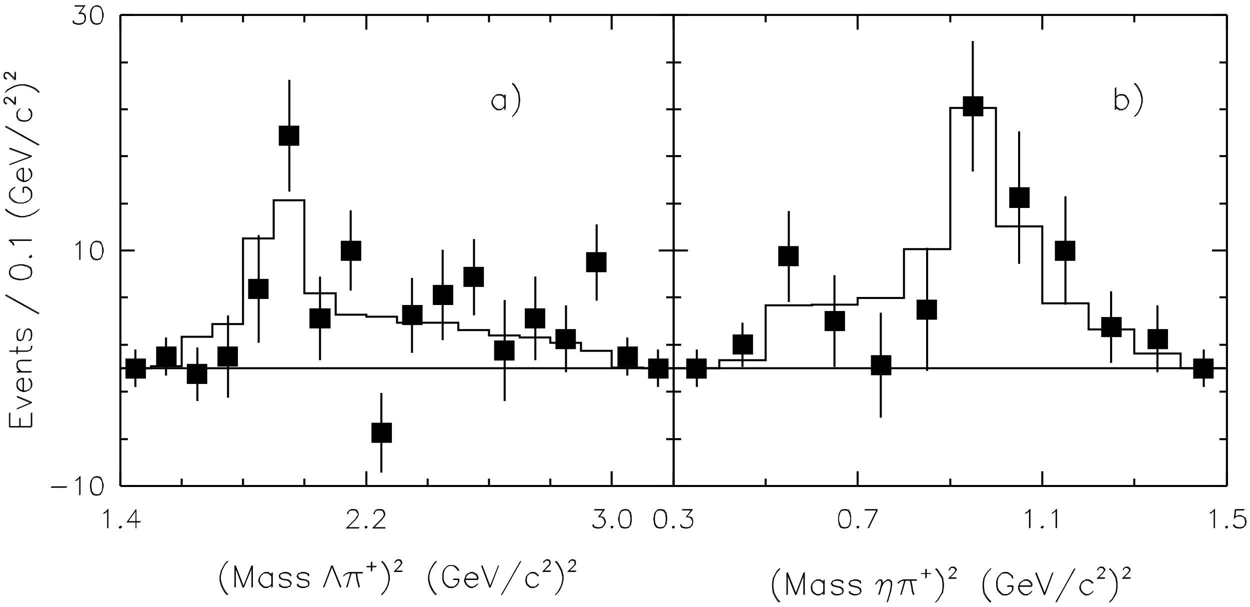


FIG. 8. Projection of Dalitz plot in the previous figure onto (a) the $M^2_{\Lambda\pi^+}$ axis and (b) the $M^2_{\eta\pi^+}$ axis

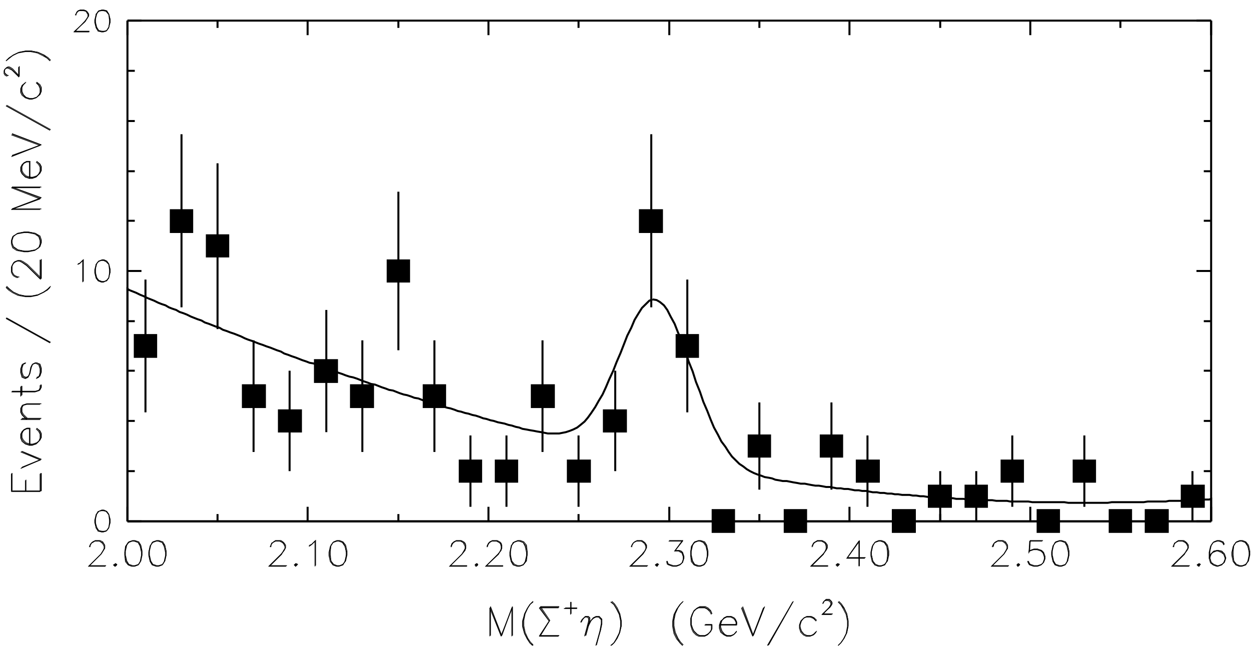


FIG. 9. Invariant mass distribution for $\Lambda_c^+ \to \Sigma^+\eta$

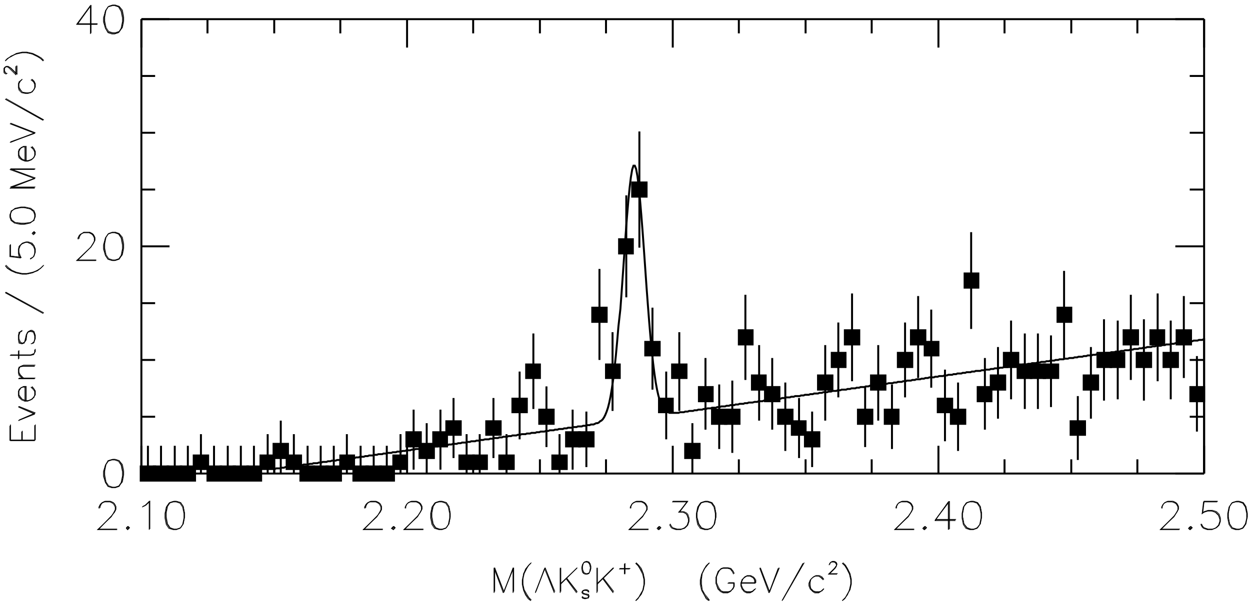


FIG. 10. Invariant mass distribution for $\Lambda_c^+ \to \Lambda K_s^0 K^+$